10-18-2021

Raman investigations of the radiation-induced modifications in iPP-VGCNF nanocomposites: The nanofillers' tale

Dorina M. Chipara
The University of Texas Rio Grande Valley, dorina.chipara@utrgv.edu

Mihail Secu

Karen Lozano
The University of Texas Rio Grande Valley, karen.lozano@utrgv.edu

Corina Secu

Mircea Chipara
The University of Texas Rio Grande Valley, mircea.chipara@utrgv.edu

Recommended Citation

Chipara, Dorina Magdalena, Mihail Secu, Karen Lozano, Corina Secu, and Mircea Chipara. 2021. "Raman Investigations of the Radiation-Induced Modifications in IPP-VGCNF Nanocomposites: The Nanofillers' Tale." Carbon Trends 5 (October): 100119. https://doi.org/10.1016/j.cartre.2021.100119.

Carbon Trends 5 (2021) 100119

Contents lists available at ScienceDirect

Carbon Trends

journal homepage: www.elsevier.com/locate/cartre

Raman investigations of the radiation-induced modifications in iPP-VGCNF nanocomposites: The nanofillers' tale

Dorina Magdalena Chipara[a], Mihail Secu[b], Karen Lozano[c], Corina Secu[b], Mircea Chipara[a,*]

[a] Department of Physics and Astronomy, The University of Texas Rio Grande Valley, 1201W. University Drive, Edinburg, TX 78539, United States
[b] National Institute for Materials Physics, Magurele, Bucharest, Romania
[c] Department of Mechanical Engineering, The University of Texas Rio Grande Valley, 1201W. University Drive, Edinburg, TX 78539, United States

ARTICLE INFO

Article history:
Received 31 July 2021
Revised 8 October 2021
Accepted 12 October 2021

Keywords:
Raman
Isotactic polypropylene
Vapor-grown carbon nanofibers
Gamma irradiation
Stress transfer
Shift of the Raman Line Position
Raman line width

ABSTRACT

Nanocomposites of isotactic polypropylene loaded by various amounts of vapor-grown carbon nanotubes ranging from 0 to 20% wt. were obtained by extrusion. Raman investigations on these nanocomposites are reported. The nanocomposites were irradiated using a ^{60}Co, with an integral dose of 1 kGy/h up to integral doses of 9 kGy, 18 kGy, and 27 kGy, in air, at room temperature. Raman measurements were performed by using a Bruker Senterra confocal Raman spectrometer operating at 785 nm. The research is focused on the information contained within the D and G Raman lines of these nanocomposites as a function of nanotube loading for various integral doses. The experimental data revealed the graduate silencing of the molecular motions assigned to the polymeric matrix due to the nanofiller and ionizing radiation.

Based on experimental data, it is concluded that the positions of the D and G lines exhibit faint shifts due to the irradiation and that (on average) these shifts are consistent with the changes of the positions of D and G lines upon the increase of the loading with vapor-grown carbon nanofibers. Raman data suggest that the irradiation relaxes the pressure exerted on the nanofiller by the polymeric matrix, indicating a path to improve the physical features of polymer-carbon nanostructure nanocomposites. The research demonstrates the capability of Raman spectroscopy to sense the modifications of molecular vibrations in polymer-based nanocomposites, for both the polymeric matrix and the nanofiller.

1. Introduction

Polypropylene (PP) is a semicrystalline polymer consisting of four crystalline phases identified as alpha, beta, gamma, and smectic [1–4]. Polypropylene (PP) has good mechanical [5], thermal [6], and radiation stability features [1,7]. The recent discovery of carbon nanostructures and, in particular of carbon nanotubes (CNTs) and carbon nanofibers (CNFs) provided a path for the improvements of the features mentioned above [8,9]. Through their very high modulus and huge aspect ratio, CNFs and CNTs enhanced the mechanical properties of the polymeric matrix (assuming a good dispersion of the nanofiller and compatible surface features [10–12]). Improvement of the thermal stability [13,6] and decreases of flammability were also reported in polymer-carbon nanostructures composites [14,12]. Additionally, the electric [15,16] and thermal conductivity of CNFs or CNTs added new features (such as thermal and electric conductivity) to the polymeric matrix. The presence of free (conducting) electrons [4] on the nanofiller provides a quick path for the delocalization of the energy deposited by the incident radiation within the nanocomposite, and for the subsequent recombination reactions of the free radicals generated within the polymeric matrix by radiation [17], thus finally improving its radiation stability.

Polymer-based nanocomposites have been obtained by dispersing various fillers such as CNTs or CNFs within different polymeric matrices [18]. The outcome is a material with a continuous phase - like a sea - represented by the polymeric matrix, with islands of nanofiller agglomerations. An important goal is to reduce the size of these agglomerations, thus increasing the contact area between the polymeric matrix and the nanofiller. The polymeric matrix accommodates the nanofiller by sacrificing its elastic features. From the mechanical point of view, the nanoparticles exert a strain on the continuous polymeric matrix. In the linear elastic domain, this strain is converted into stress via the multiplication by the Young modulus. For PP the Young modulus is ranging from 400 $\times$ 10^6 Pa

* Corresponding author.
E-mail address: mircea.chipara@utrgv.edu (M. Chipara).

https://doi.org/10.1016/j.cartre.2021.100119

[9,19], up to about 1.6 × 10^9 Pa (for neat PP at a strain rate of 0.05%min^{-1} [5]), thus providing impressive stress for the actual strain due to the nanofiller. For whatever reason, the report on the study of mechanical properties of PP loaded by single-walled carbon nanotubes (SWCNTs) by Raman spectroscopy did not include the analysis of the stress or strain on the position and/or width of the main D and G bands [9]. The tangent modulus for unstrained fibers of PP was estimated to be about 4.0 × 10^9 Pa [20]. In the case of isotactic polypropylene (iPP) loaded by CNFs, the position of the G band was moved to larger shifts as the strain applied was increased [21]. This shift was linear for strains less than 2%. The dependence of the G band on applied strain was accurately described by [21]:

$$\varepsilon(x) = [\nu(x) - \nu(0)]/S \quad (1)$$

where ε(x) is the strain associated with the position identified by the one-dimensional coordinate x, $\nu(0)$ is the position of the G line assuming that no strain is acting on the nanofiber, ν(x) is the position of the nanofiber if a strain of x% is acting on it, and S is the slope of the dependence of the Raman line G on the strain. It was reported that for PP – CNFs, S is equal to 11.9 cm^{-1}/% (assuming that ν is measured in cm^{-1} and ε in%) [21].

The nanofiller senses the pressure (stress) σ_F exerted by the polymeric matrix. This stress is eventually equal and opposite to the stress acting on the polymeric matrix, σ_P. However, the associated stress acting on the nanofiber (in the linear elastic range) is converted into the strain ε_F via a division by the Young modulus of the nanofiller. For CNFs, the Young modulus ranges typically between 10^{11} and 10^{12} Pa [19]. This qualitative description suggests that the strain acting on the CNFs or CNTs dispersed within typical polymeric matrices is smaller than the strain exerted on the polymeric matrix by about 2 to 3 orders of magnitude. From the mechanical point of view, the CNFs are in a quasi-isostrain domain, where changes of the applied stress are not sustained by sizable modifications of the strain. As the nanofiller concentration increases, the polymeric matrix is stretched up to the failure point where the nanofillers' bleeding starts. This range corresponds to the break of the polymer in a standard stress-strain dependence.

Raman spectroscopy evolved into a powerful method for investigating atomic and molecular motions within matter. Consequently, it is expected that the development of internal stresses (strains) may be sensed and monitored by both Raman and FTIR spectroscopies [22]. Raman spectroscopy may sense both the polymeric matrix and the nanofiller (in polymer-based nanocomposites), providing complex and rich information [22,23].

Raman spectroscopy of carbon nanostructures focuses typically on three spectral ranges:

1. Low wavenumber range (typically below 500 cm^{-1}). Within the low wavenumber range, the Raman spectra of carbon nanostructures typically include various radial breathing modes associated with vibrations of closed atomic contour. The Radial Breathing Modes (RBMs) were reported in SWCNTs and double-walled carbon nanotubes [24]. Essentially, multi-walled carbon nanotubes (MWCNTs), CNFs, and carbon fibers (CFs) do not exhibit well-resolved RBM spectra, although a broad Raman line maybe eventually noticed [11,24].
2. Medium wavenumbers (or DG) range typically extends from 1200 cm^{-1} to 1700 cm^{-1} and includes two strong and well-resolved lines; one located within the range 1250 to 1450 cm^{-1} and identified as *D* band (originating from defects [25]) and the other located in the range 1500 to 1650 cm^{-1}, labeled as *G* band, and assigned to graphitic structures [24]. The position of the *D* band typically ranges between 1360 and 1365 cm^{-1} [26]. The position of the *D* band is moved to larger Raman shifts as the energy (frequency) of the impinging Raman radiation is increased [26]. Raman investigations on CNFs subjected to mechanical stresses (strains) indicated that the parameters of the *D* and *G* lines (line position, line width, and the ratio between the area of the *D* line and the area of the *G* line, labeled as S_D/S_G) are sensitive to local stresses (strains).

It was reported [27] that the position of the D band shifts to smaller Raman shifts as the strain acting on the CNTs is increased (extension mode). The dependence was reported to be almost linear with a slope of about −4.7 [1/(cm%strain)] [27].

The position of the G line is usually reported in the range 1585 to 1900 cm^{-1} [24,26]. In some instances, the G line is split into up to three components labeled as G^+, G-, and G^{-2}, with G^+ located at larger Raman shifts than the main G line and G^- (as well as G^{-2}) located at lower Raman shifts than the main *G* line [26]. It was reported that the position of the G^+ line (ν_{G+}) does not depend on the diameter of the nanotube while the position of the G^- line (ν_{G-}) depends on the diameter of the nanotube d, according to [25]:

$$\nu_{G^-} = \nu_{G+} - A/d^2 \quad (2)$$

Where A = 79.5 × 10^{-7} nm for metallic and respectively 47.7 × 10^{-7} nm for semiconducting samples. Typically both G^+ and G^- lines are noticed in metallic and semiconducting nanotubes [25]. The splitting of the G line under stress was also reported [8]. The SWCNTS' Raman shift for D, G^+, and G^- components were reported to move towards smaller values as the applied strain was increased [27].

For SWCNTs subjected to strains up to 5% the average slope for the displacement of the D band was −4.7 [1/(cm%strain)], for the G^+ band was −8.6 [1/(cm%strain)], and for the G- band was −8.0 [1/(cm%strain)] [27,28]. Slightly larger slopes were reported for SWCNTs [29]. The general conclusion was that compressive stress increases the value of the Raman shift and tensile stress decreases the value of the Raman shift.

A natural (analogous) model for the effect of stress/strain on nanotubes is provided by the Raman studies on CNTs and CNFs subjected to high pressures [30–33],. Thus the increase of the pressure up to 140 GPa moved the position of the G Raman line towards larger values [33]. The displacement was linear with slopes of 5.8[1/(cmGPa) for SWCNTs and 4.3[1/(cmGPa) for SWCNTs for pressures up to 10 GPa [34].

3. High wavenumber range typically extends from 2300 to 3600 cm^{-1}. This range includes the G' (2D or D*) line located at about 2700 cm^{-1}. These lines generally are weaker than the D and G lines for carbon nanofibers [24]. Usually, the G' line appears to be more sensitive to stresses/strains; however, the analysis of its parameters may involve more significant errors due to its reduced intensity and the overlap with additional Raman lines originating from the matrix. No contributions due to the nanofiller were recorded in this spectral range for incoming electromagnetic radiation of 785 nm, within experimental errors.

Previous experimental data [35] reported that the intensity of the D line is not affected by irradiation (within experimental data); the positions of the D and G lines are not affected by gamma irradiation up to integral doses of about 500 kGy. The intensity of the G line increases as the integral dose is increased [35]. Studies on electron beam irradiated MWCNTs indicated that the ratio between the area of the D and G bands is not affected by irradiation (within experimental errors), revealing a displacement towards smaller Raman shifts for the D line as the integral dose was increased up to 1000 kGy [36]. The position of the G band appeared to be less sensitive on the integral dose [36]. Studies on the effect of gamma irradiation in air on composite of

polyethylene (PE) loaded by up to 1% VGCNF revealed that the oxidation index is decreased by the presence of MWCNTs. However, the oxidation index is decreased as the irradiation (integral) dose is increased, suggesting that the defects generated by the irradiation of nanotubes have an antioxidant behavior improving the radiation stability of the polymeric matrix [37]. Electron beam irradiated VGCNF (from the same company) revealed minimal modifications due to irradiation; the initial position of the D and G band (located at 1350.72±1.06 cm^{-1} and respectively at 1590.80 ± 1.5 cm^{-1} are shifted to 1352.41 ± 0.94 cm^{-1} and respectively1590.22 ± 1.09 cm^{-1} after irradiation up to an integral dose of 1000 kGy (including heating) and to 1351.83 ± 0.9 cm^{-1} and respectively 1590.37 ± 1.03 cm^{-1} after heating and irradiation up to 3000 kGy [38]. The ratio between the areas of the D and G bands was increased from 3.67 ± 0.07 to 3.70 ± 0.10 after irradiation (and heating) at up to 1000 kGy and to 3.72 ± 0.09 after irradiation (and heating) up to 3000 kGy [38]. The heating temperature was about 350 °C and thus was too low to trigger modifications of the VGCNFs [38].

This manuscript reports on the Raman investigations of a series of nanocomposites obtained by adding Vapor Grown Carbon Nanofibers (VGCNFs) to a polymeric matrix (iPP). The loading with VGCNFs was ranging between 0 and 30% wt. VGCNF. Additionally, the effect of ionizing radiation on these samples is discussed in detail. The analysis focuses on the fillers' tale, with emphasis on the region of the Raman spectrum located between 1200 and 1700 cm^{-1}. Usually, the research on the molecular vibrations in polymer-based nanocomposites is focused either on the vibrations originating from the polymeric matrix [39] or on the vibrations assigned to the nanofiller [39–41]. This research demonstrates the capability of Raman spectroscopy to sense the modifications of molecular vibrations in polymer-based nanocomposites, for both the polymeric matrix and the nanofiller, and completes our previous study on the changes in the Raman spectra of the polymeric matrix due to the irradiation and loading by VGCNFs in the same samples [23].

2. Experimental methods

High shear mixing of isotactic polypropylene (Marlex HLN-120–01; Philips Sumika Polypropylene Company) with carbon nanofibers (PR-24AG; Pyrograf Products, Inc) was used to produce nanocomposites of isotactic polypropylene loaded by vapor grown carbon nanofibers (iPP-VGCNF), by utilizing a HAAKE Rheomix operating at 65 rotations per minute (rpm) and 180 °C for 9 min followed by an additional mixing at the same temperature and at 90 rpm for 5 min. The loading of the polymeric matrix ranged between 0 and 20% wt. The final samples were obtained by hot pressing the as obtained blends into sheets with a thickness of 0.6 mm by a force of 1000 N for 100 s, at 180 °C. The as-obtained samples were gamma-irradiated in air, at room temperature at a dose rate of 1 kGy/h up to integral doses of 0 (reference sample), 9 kGy, 18 kGy, and 27 kGy by a ^{60}Co source. The Raman measurements were performed about one month after irradiation. After the irradiation was stopped, the irradiated samples were stored in sealed plastic bags at room temperature.

Raman measurements have been performed using a Bruker Senterra dispersive Raman microscope spectrometer equipped with a 785 nm laser diode.

The subsequent analysis will focus on the spectral parameters of VGCNFs. The analysis will dissect the effect of the polymeric matrix and of the ionizing radiation on the whole nanocomposite while isolating the effect on the nanofiller (VGCNF) component. This will provide a basis for a better understanding of the atomic and molecular elasticity in polymer-based nanocomposites. In addition, complementary data by Raman spectroscopy on the effect of ionizing radiation and loading by VGCNFs on the position and widths of some relevant Raman lines originating from the polymeric matrix have been reported [23].

3. Experimental results

The as recorded, full Raman spectra in the range 200 to 3200 cm^{-1} for iPP-VGCNF nanocomposites, irradiated up to various integral doses are collected in Fig. 1. At low loading with VGCNFs (less than 5% wt. VGCNFs) the Raman spectrum contains both the spectra assigned to the polymeric matric (iPP) as well as the spectra assigned to VGCNFs. As the loading with VGCNFs increases, the Raman lines due to the polymer are silenced and eventually broadened (Fig. 1). Typically for nanocomposites containing more than 5% VGCNFs, the Raman spectrum is dominated by the contributions originating from the nanofiber.

As noticed from Fig. 1, in agreement with Raman data on VGCNFs [25,24], no Raman line was detected in the low wavenumber region. In the medium wavenumber range (Fig. 2), at high loading with VGCNs (above 5.0% wt. VGCNF), the Raman spectrum is dominated by the *D* and *G* lines.

The Raman spectra of iPP-VGCNF nanocomposites irradiated up to different integral doses ranging from 0 to 27 kGy, loaded by various weight concentrations of VGCNFs, and analyzed in 1200 to1700 cm^{-1} range, are shown in Fig. 2.

The following Raman lines were observed and identified in the range 1200 to 1700 cm^{-1} (Table 1).

A simple analysis of the spectra collected in Fig. 1 reveals the strong modifications generated by the loading with VGCNFs. It is noticed that the addition of the nanofiller silences the molecular vibrations occurring within the polymer. At high loading with nanofiller, the spectra of these nanocomposites are dominated by the spectrum of the nanofiller.

The Raman lines assigned to the polymeric matrix are relatively weak, and they are decaying fast as the loading with VGCNFs. is increased. Typically, the Raman spectra of the nanocomposites are dominated by the lines due to the nanofiller for nanocomposites containing 5% or more VGCNFs, irrespective of the integral irradiation dose.

The Raman spectra of iPP-VGCNFs in the range 1200 to 1700 cm^{-1} consists of up to 7 lines, with two lines associated to the D band originating from VGCNFs (at low wavenumbers, 1300 cm^{-1}) and to the G band, originating also from VGCNFs and located at the high wavenumber limit, at about 1600 cm^{-1}. Up to 5 weak Raman lines originating from the polymeric matrix were noticed between the *D* and *G* lines.

$$
\begin{aligned}
I = {} & (2*A_1/\pi)*W_1/4*(x-C_1)*(x-C_1)\\
& +W_1*W_1+(2*A_2/\pi)*(W_2/(4*(x-C_2)*(x-C_2)+W_2*W_2))+\\
& +(2*A_3/\pi)*(W_3/(4*(x-C_3)*(x-C_3)+W_3*W_3))\\
& +(2*A_4/\pi)*(W_4/(4*(x-C_4)*(x-C_4)+W_4*W_4))+\\
& +(2*A_5/\pi)*(W_5/(4*(x-C_5)*(x-C_5)+W_5*W_5))\\
& +(2*A_6/\pi)*(W_6/(4*(x-C_6)*(x-C_6)+W_6*W_6))\\
& +(2*A_7/\pi)*(W_7/(4*(x-C_7)*(x-C_7)+W_7*W_7))\\
& +B+S*x+Q*x*x;
\end{aligned}
\tag{3}
$$

Where I is the intensity of the as-recorded spectrum, A_i is the individual intensity of each line, C_i, the position (peak) for each line, W_i is the width for each line, B is the base correction, S is the slope correction, and Q is the quadratic corrections (for all these lines). The subscript "i" takes values between 1 and 7, corresponding to each Raman line component. Eq. (3) provides an excellent experimental data fit, with correlation coefficients better than 0.95. The best-fit parameters generated the values for lines positions, widths, (relative) amplitudes, and area ratio.

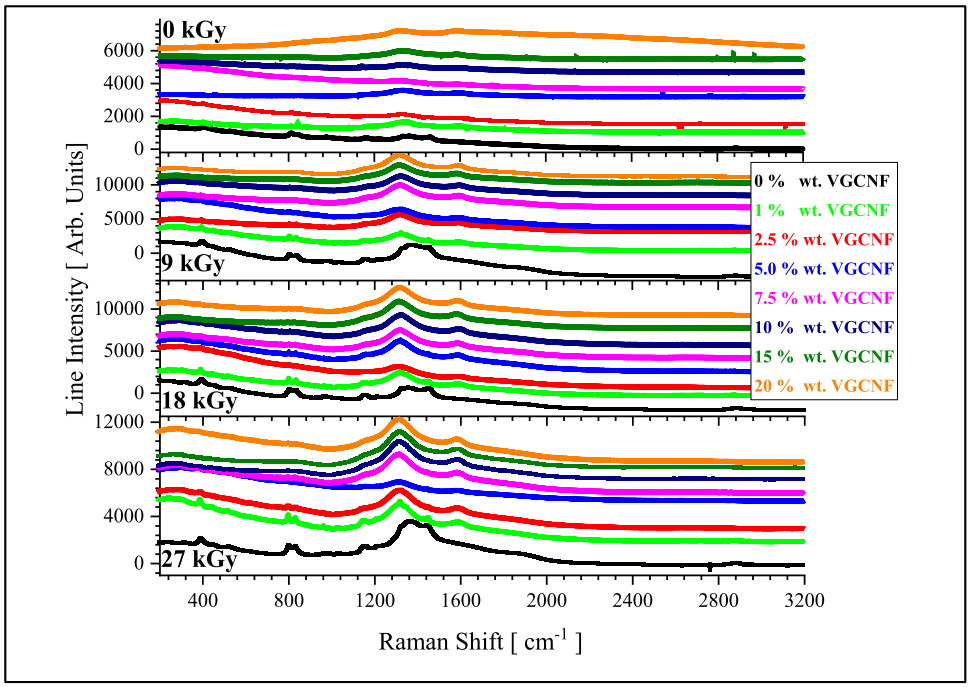

Fig. 1. Raman spectra of various iPP-VGCNF irradiated at different integral doses ranging between 0 and 27 Gy.

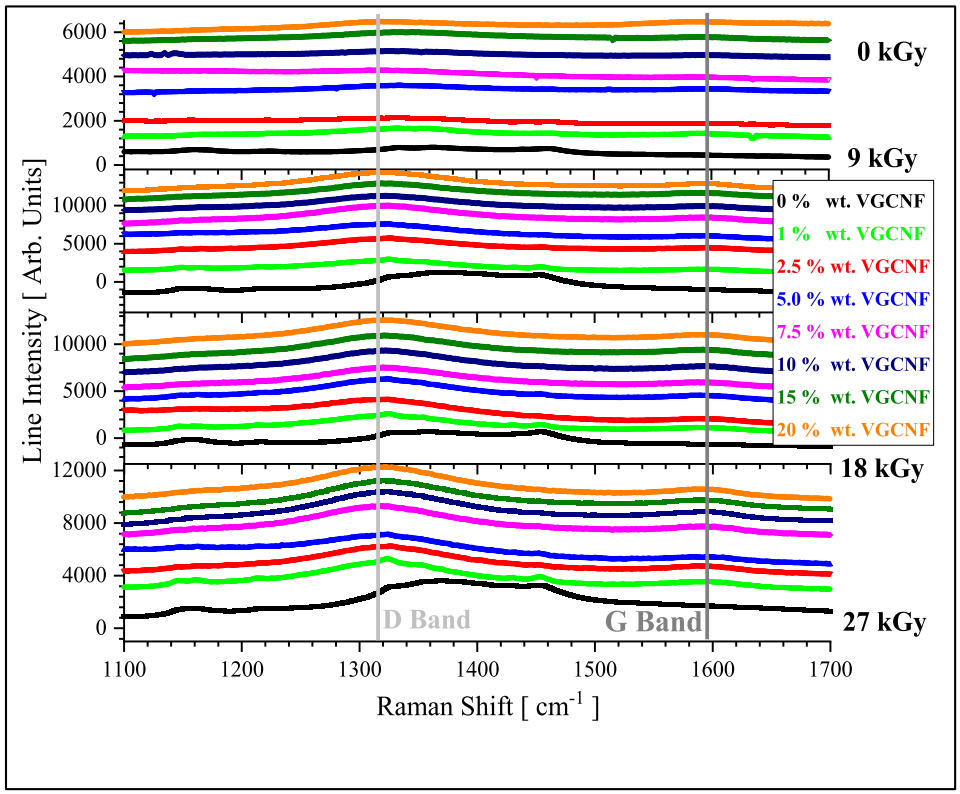

Fig. 2. Detail of Raman spectra showing the *D* and *G* bands for various iPP-VGCNF irradiated at different integral doses ranging between 0 and 27 Gy.

The upper panel of Fig. 3 depicts the effect of various loadings with VGCNFs on the position of the *D* line for different integral doses. For the unirradiated samples, the positions of the *D* line are shifted downwards as the concentration of VGCNFs is increased. At each constant (not zero) dose rate, the position of the D line was independent on the concentration of VGCNFs. It was noticed that the average position of the D line (for all concentrations of the nanofiller, at a given integral dose) shows a faint shift towards smaller Raman shifts as the integral dose is increased.

The lower panel of Fig. 3 represents the dependence of the position of the *D* line on the integral dose, for various loadings with VGCNFs. Excepting the samples containing 20% VGCNFs, the position of the *D* line exhibits a small downward displacement as the integral dose is increased. The sample containing 20% wt. VGCNFs

Table 1
Main Raman lines located between 1200 and 1700 cm^{-1} (for both the polymeric matrix and the nanofiller).Table 1

	Position [cm^{-1}]	Source	Nature	Reported Position [cm^{-1}]	Ref	*
1	1220	Polymeric Matrix	tCH_2+vC–C+dCH	1220	[23,42,43]	
1		Polymeric Matrix	tCH_2+wCH+v(C–C)	1220	[44]	
2	1250	Polymeric Matrix	dCH+tCH_2+rCH_3	1257	[42]	
3	1335	Nanofiller	*D* Line	1308–1360	[24]	
4	1365	Polymeric Matrix	CH_3 symmetric bending+SCH	1360	[45]	
5	1440	Polymeric Matrix	dCH_3 asymmetric	1435	[45]	S
6	1457	Polymeric Matrix	dCH_3 asymmetric+dCH_2	1457	[46]	
6	1465	Polymeric Matrix	dCH_3 asymmetric+dCH_2	1457	[23]	
7	1600	Nanofiller	G Line	1500–1600	[24]	

v= stretching; *d* = bending; *r*=rocking; *t*=twisting; *a*=amorphous; *c* =crystalline; *s*=amorphous.

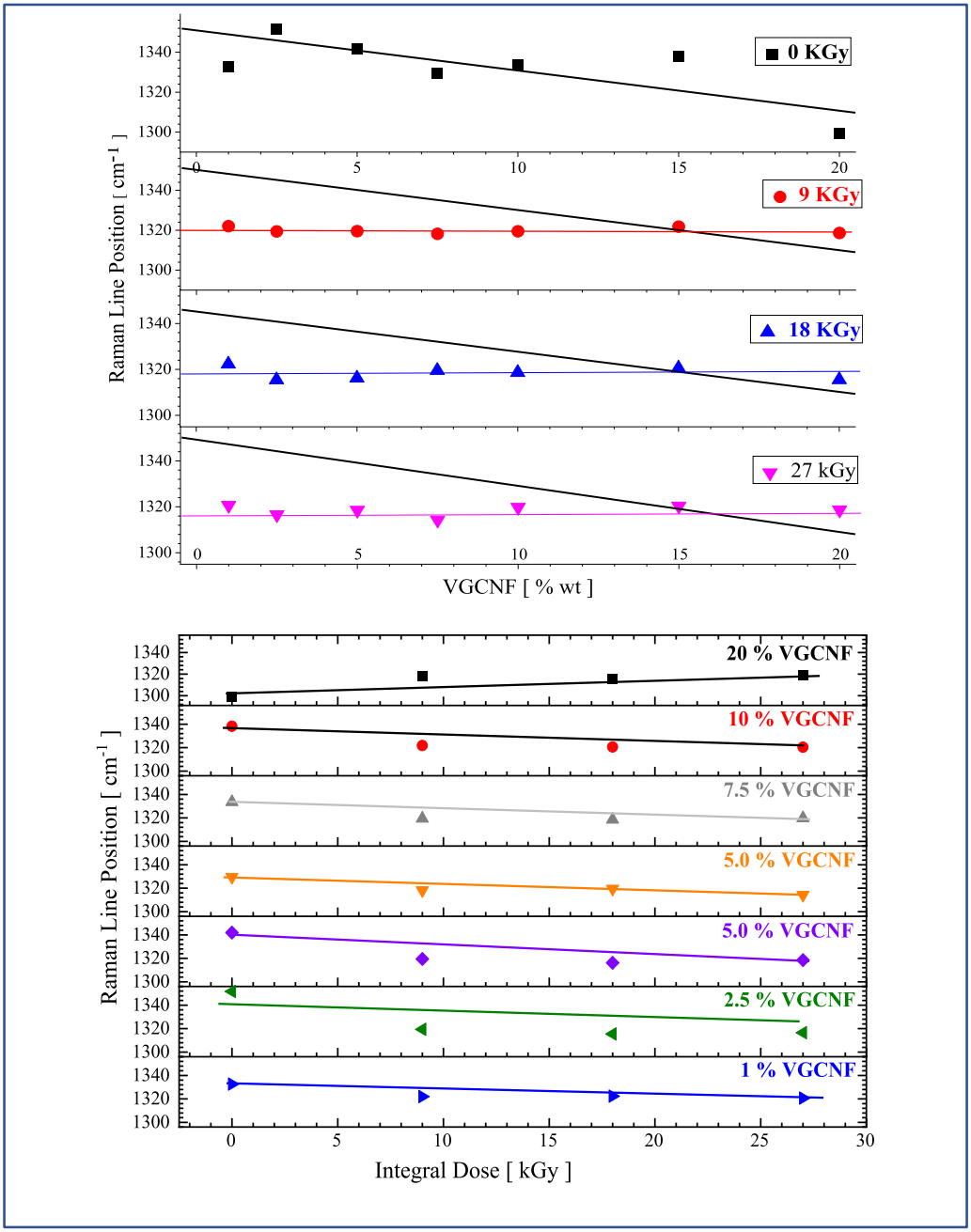

Fig. 3. The dependence of the position of the *D* band (originating from VGCNF dispersed within iPP) on: UPPER PANEL the loading by VGCNF at various integral doses. LOWER PANEL: the integral dose for various loadings with VGCNF.

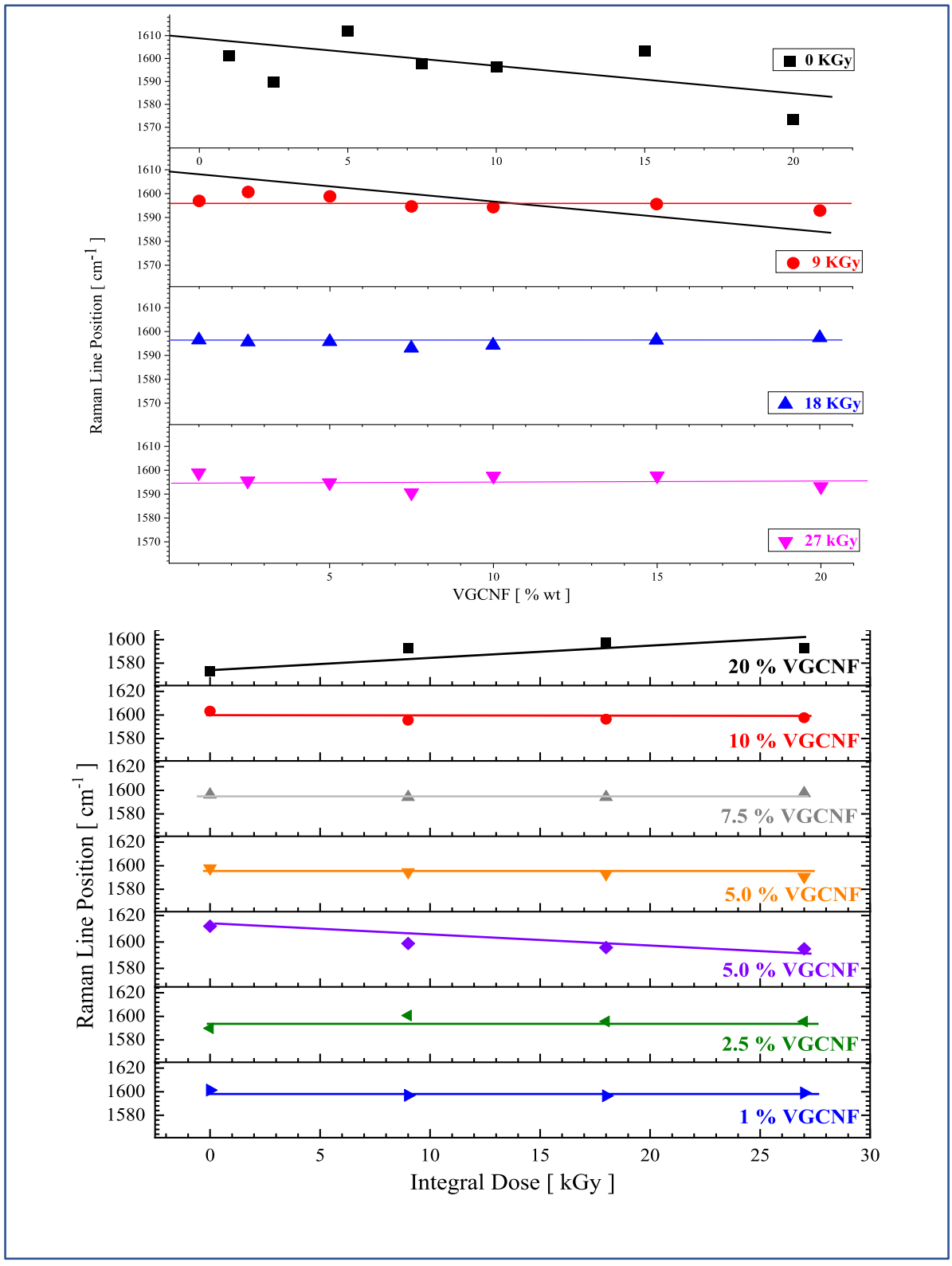

Fig. 4. The dependence of the position of the *G* band (originating from VGCNF dispersed within iPP) on: UPPER PANEL the loading with VGCNFs for different integral doses and LOWER PANEL: the integral dose for various loadings with VGCNFs.

exhibits an upward shift of the *D* line as the integral dose was increased.

The upper panel of Fig. 4 represents the position of the *G* line as a function of the loading by VGCNFs for different integral doses. It is noticed that for the not irradiated samples, the position of the *G* line moves towards smaller Raman shifts as the concentration of the VGCNFs is increased. For all irradiated samples, it was concluded that for each integral dose, the position of the G line is essentially not affected by the loading with VGCNFs. As in the previous case, the average (over all concentrations of nanofillers)

position of the *G* band, for constant integral dose, exhibits a faint decrease as the integral dose was increased.

The lower panel of Fig. 4 represents the dependence of the position of the *G* line on the integral dose, for various loadings with VGCNFs. Excepting the samples containing 5% wt. VGCNFs and 20% VGCNFs, the position of the G line does not appear to be affected by the integral dose. The sample with 5% VGCNF shows a very small decrease of the G line position as the integral dose is increased. The sample containing 20% wt. VGCNFs exhibits an upward shift of the G line position, suggesting similar effects for irradiation and loading with nanofiller for both D and G lines.

The dependence of the width of the *D* line on the loading by VGCNFs for various integral doses is shown in the upper panel of Fig. 5. It is observed that the D line's width experiences weak displacements towards higher Raman shifts as the concentration of VGCNFs is increased, for all investigated samples (irradiated and not irradiated). The D line's width (see the lower panel of Fig. 5) does not depend on the integral dose for all samples excepting the one loaded by 20% VGCNFs, which exhibits a moderate upwards shift as the integral dose is increased.

The upper panel of Fig. 6 depicts the dependence of the width of the *G* band originating from VGCNFs dispersed within iPP on loading with VGCNFs, for different integral doses. It is observed that the width of the G band is gently broadened as the loading by VGCNFs is increased. The width of the *G* line is not affected by the gamma irradiation within the experimental errors. The lower panel of Fig. 6 represents the width of the *G* band as a function of integral dose for various loadings by VGCNFs. It is noticed that for constant loadings with the nanofiller, the width of the G line does not depend on the integral dose.

The upper panel of Fig. 7 depicts the dependence of the ratio between the area of the *D* and *G* areas on the loading by VGCNFs, for various integral doses. It is concluded that for each integral dose the ratio S_D/S_G is almost independent of the loading by VGCNFs. The dependence of the S_D/S_G on the integral dose at various loading with VGCNFs exhibits a weak increase as the integral dose is increased, for samples loaded by 0, 1, and 20% wt. VGCNFs (see the lower panel of Fig. 7). For all the other samples, the ratio S_D/S_G is constant (within experimental errors).

4. Conclusions

Based on reported studies on the effect of ionizing radiation up to 1000 KGy (analyzed within the introduction) it was expected a negligible impact of the gamma irradiation on the Raman spectra of VGCNFs (for such low integral doses - up to 27 KGy). The experimental data supported these expectations; the reported effect of ionizing radiation on the positions and widths of the D and G lines was significantly weaker than the effect of the loading by VGCNFs. However, both the increase of the integral dose and the increase of the loading with VGCNFs generated the same modifications.

The detailed analysis of the average positions for both D and G lines of all samples irradiated at a constant integral dose revealed that qualitatively both the irradiation and the loading by VGCNFs are acting cooperatively, by shifting the line positions downwards.

The most intriguing and important conclusion of this study is that the dependence of the Raman line parameters on the loading by VGCNFs tends to be erased by the ionizing radiation. This suggests that the ionizing radiation provides a path for the relaxation of the polymeric network. Such observation may have important consequences in the production of nanocomposites based on CNTs and CNFs.

A final point related to the research proposed is connected to the sign of the Raman shift. The simple rule of thumb discussed within the introduction would identify the tensile strain with the downward displacement of the Raman line and the compression strain with the upwards shift. It was expected that due to the compressive pressure exerted on VGCNFs the positions of the D and G line should be displaced towards larger Raman shifts. Unfortunately, the answer is more complex mostly due to three competing elements.

1 Compression or extension? The analysis of experimental data of nanofiller within polymeric matrix is complicated by the mass conservation (for both the nanofiller and the polymeric matrix), via the Poisson ratio as stretching a sample along a direction generates its contraction within a perpendicular plane. Usually, the change in the density of the sample is not capable of balancing the change of the volume due to the applied stress. Consequently, it appears that the dissemination between compression and tensile strains is not very simple. For example, in the uniaxial stretching of polyethylene, the lines located at 1460 and 1480 cm^{-1} are moving towards larger Raman shifts as the strain is increased (for strains below 100%) while (in the same sample) the line located at 1080 cm^{-1} exhibit the opposite dependence in the same range of strains [47].

2 The behavior of the VGCNFs dispersed within the iPP matrix is analogous to the behavior of carbon nanostructures subjected to hydrostatic pressure. The pressure dependence of the Raman line position of the D line, ν_D, in diamond was demonstrated to obey the equation [48]:

$$\nu_D = \nu_D^{(0)} + AP + BP^2 \quad (4)$$

Where $\nu_D{}^{(0)}$ represents the position of the D line in diamond in the absence of any pressure (1330 cm-1), $A = 2.83$ [1/(cmGPa)] and $B = -3.65 \times 10^{-3}$ [1/(cmGPa)] [48]. Because B is negative, the actual displacement of the position of the D line is negative if $A < 2BP$ and positive for $A > 2BP$. Hence, for very small pressures, the actual position of the D line is displaced to smaller values than that of the free diamond). A similar mechanism in VGCNF may eventually explain the unexpected sign of the displacement o the line positions for both *D* and *G* lines.

1 The behavior of actual polymer-based nanocomposites. Some recent studies focused on the correlation between the elastic features of polymer nanocomposites (as shown by the stress-strain dependence) and the parameters of the Raman lines. For graphene and graphene dispersed within polymethylmethacrylate (PMMA), the positions of the G and 2D lines were demonstrated to be displaced towards lower values as the applied strain was increased [8], thus supporting our results. The nicest example comes from the combined Raman and mechanical investigation of SWCNTs dispersed within PMMA that demonstrated that for the G line, the increase of stress/strain applied to the nanocomposite results in a displacement downwards of the position of the G band (for small strains and within the linear elastic range) (see Fig. 5 of [28]). Within th ultimate strength domain the position of the G line starts to be displaced weakly upwards as the strain is increased. Formally this supports a non-linear dependence of the Raman line position on strain, somehow analogous to the previous scenario.

The changes revealed by the Raman investigations of the effect of irradiation by gamma rays or loading with VGCNFs on the Raman lines assigned to the nanofibers are supported by the Raman data originating from the polymeric matrix. It was reported [23] that the main Raman lines originating from the polymeric matric (iPP) were also displaced towards a smaller wavenumber, indicating that the strain of the polymeric matrix is enhanced by irradiation. The competition between the irradiation generated modifications of the Raman spectra (positions) and the effect of loading with VGCNFs was also noticed from the study of the Raman analysis of the lines originating from the polymer. A slightly larger

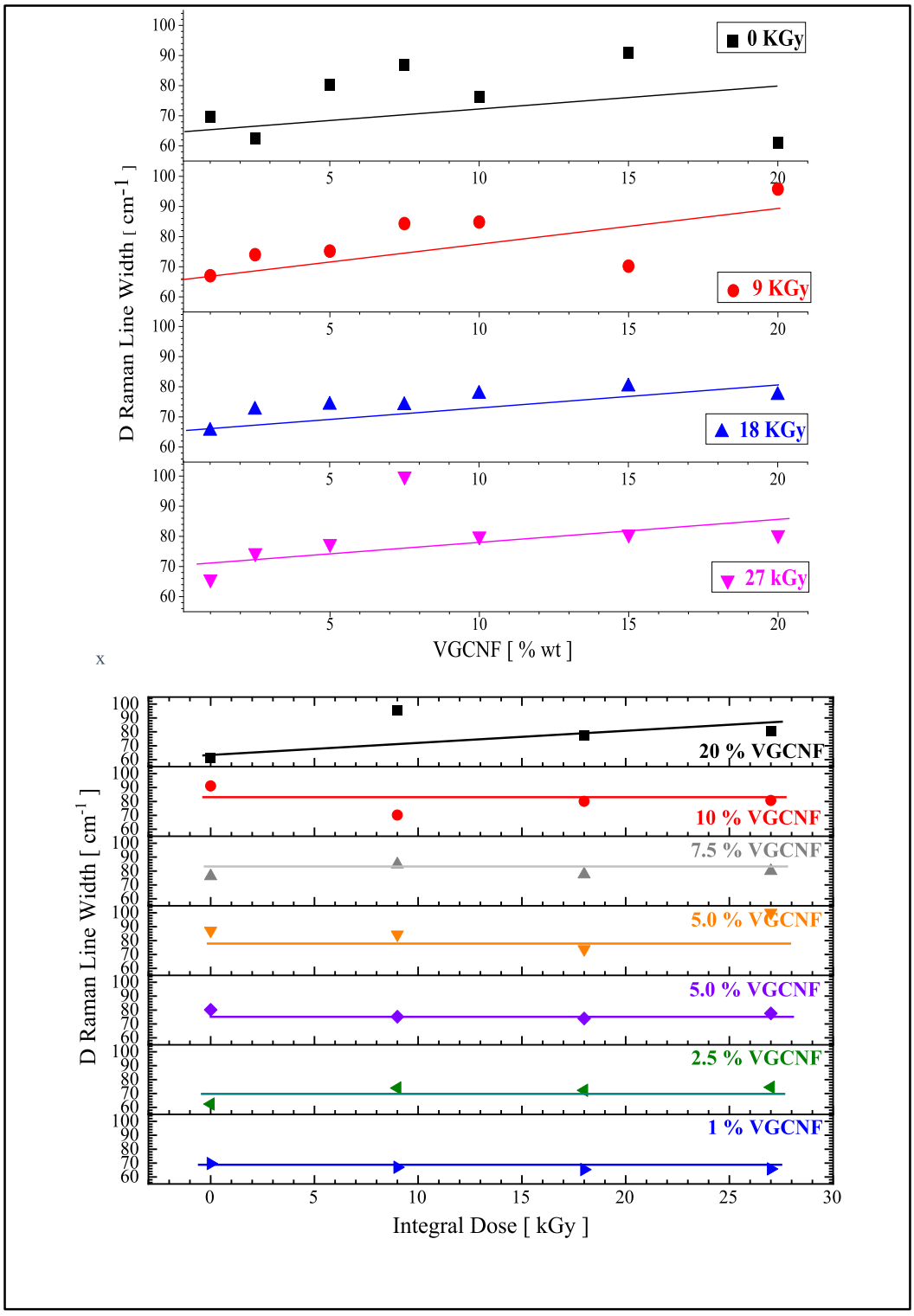

Fig. 5. The dependence of the width of the *D* band (originating from VGCNF dispersed within iPP) on: UPPER PANEL the loading by VGCNF at various integral doses and LOWER PANEL the integral dose for various loadings with VGCNFs.

strain was reported [23] within the amorphous domains, based on the Raman displacement.

A sudden change in the dependence of the shift of Raman line positions as a function of integral dose for samples loaded by 10 and 20% VGCNF was noticed and eventually related to the swift deterioration of the nanocomposite. Based on existing literature data, the transition involves shifts of the order of 20 cm^{-1} (for the D line), corresponding to a strain of about 2.5%. Assuming for nanofibers a Young modulus of 0.2 TPa [49], the estimated stress acting on the VGCNF is of the order of 5 MPa.

5. Declaration of Competing Interest

The authors declare that they have no known competing financial interests or personal relationships that could have appeared to influence the work reported in this paper.

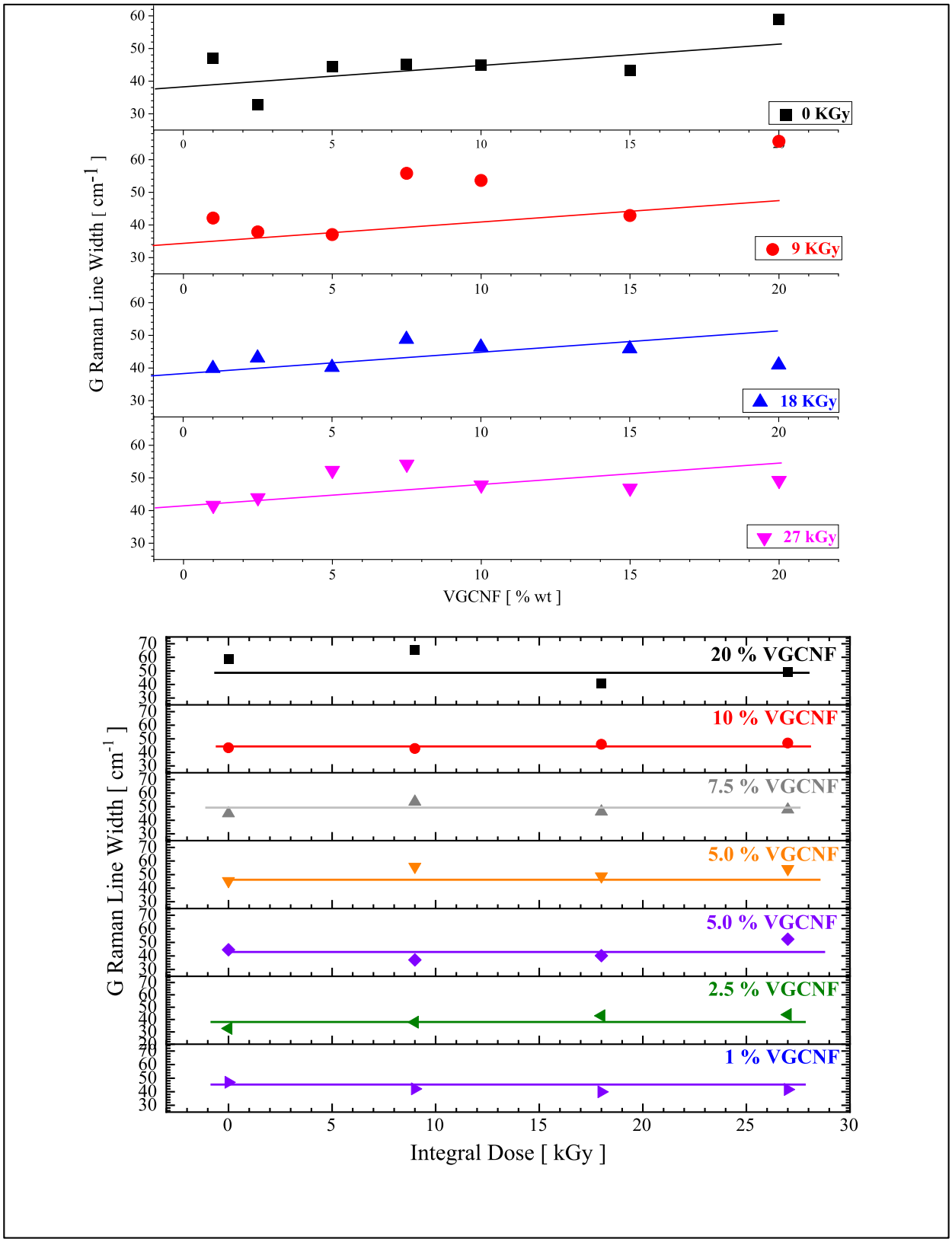

Fig. 6. The dependence of the width of the *G* band (originating from VGCNF dispersed within iPP) on UPPER PANEL the loading by VGCNF at various integral doses and LOWER PANEL: the integral dose for various loadings with VGCNFs.

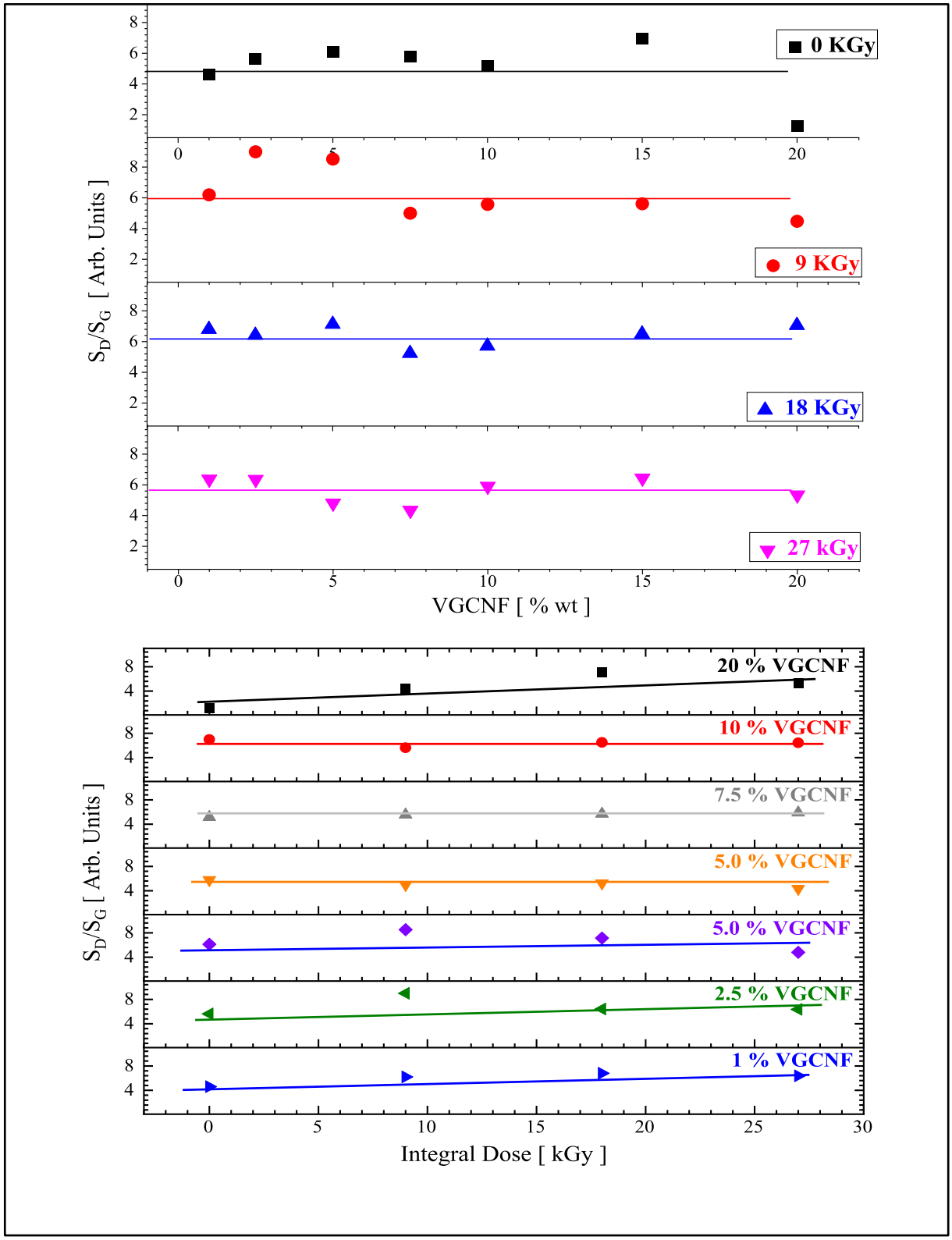

Fig. 7. The dependence of the ratio S_D/S_G for VGCNF dispersed within iPP on UPPER PANEL the loading by VGCNF at various integral doses and LOWER PANEL:the integral dose for various loadings with VGCNFs.

Acknowledgments

This research was supported by the NSF PREM award under grant No. DMR-1523577: UTRGV-UMN Partnership for Fostering Innovation by Bridging Excellence in Research and Student Success, and by the DOD. Grant W911NF-15–10063 "Raman Spectrometer for the Characterization of Advanced Materials and Nanomaterials," awarded to University of Rio Grande Valley, and the support of IRASM center of Irradiation Technology, "Horia Hulubei" National

Institute for Physics and Nuclear Engineering (NIPNE), where the samples irradiation has been performed.

References

[1] D.E. Gen, K.A. Prokhorov, G.Y. Nikolaeva, E.A. Sagitova, P.P. Pashinin, B.F. Shklyaruk, E.M. Antipov, Raman spectra of various polymorphs of isotactic polypropylene, Laser Phys. 21 (2011) 125–129, doi:10.1134/s1054660x11020010.

[2] C. Angelloz, R. Fulchiron, A. Douillard, B. Chabert, R. Fillit, A. Vautrin, L. David, Crystallization of isotactic polypropylene under high pressure (γ phase), Macromolecules 33 (2000) 4138–4145, doi:10.1021/ma991813e.

[3] R. Thomann, C. Wang, J. Kressler, R. Muelhaupt, On the γ-phase of isotactic polypropylene, Macromolecules 29 (1996) 8425–8434, doi:10.1021/ma951885f.

[4] M. Chipara, J.R. Villarreal, M.D. Chipara, K. Lozano, A.C. Chipara, D.J. Sellmyer, Spectroscopic investigations on polypropylene-carbon nanofiber composites. I. Raman and electron spin resonance spectroscopy, J. Polym. Sci. Part B Polym. Phys. 47 (2009) 1644–1652, doi:10.1002/polb.21766.

[5] Y. Zhou, V. Rangari, H. Mahfuz, S. Jeelani, P.K. Mallick, Experimental study on thermal and mechanical behavior of polypropylene, talc/polypropylene and polypropylene/clay nanocomposites, Mater. Sci. Eng. A 402 (2005) 109–117, doi:10.1016/j.msea.2005.04.014.

[6] M. Chipara, K. Lozano, A. Hernandez, M. Chipara, TGA analysis of polypropylene-carbon nanofibers composites, Polym. Degrad. Stab. 93 (2008) 871–876, doi:10.1016/j.polymdegradstab.2008.01.001.

[7] A.T. Fintzou, M.G. Kontominas, A.V. Badeka, M.R. Stahl, K.A. Riganakos, Effect of electron-beam and gamma-irradiation on physicochemical and mechanical properties of polypropylene syringes as a function of irradiation dose: study under vacuum, Radiat. Phys. Chem. 76 (2007) 1147–1155, doi:10.1016/j.radphyschem.2006.11.009.

[8] D.G. Papageorgiou, Z. Li, M. Liu, I.A. Kinloch, R.J. Young, Mechanisms of mechanical reinforcement by graphene and carbon nanotubes in polymer nanocomposites, Nanoscale 12 (2020) 2228–2267, doi:10.1039/c9nr06952f.

[9] T.E. Chang, L.R. Jensen, A. Kisliuk, R.B. Pipes, R. Pyrz, A.P. Sokolov, Microscopic mechanism of reinforcement in single-wall carbon nanotube/polypropylene nanocomposite, Polymer 46 (2005) 439–444 (Guildf), doi:10.1016/j.polymer.2004.11.030.

[10] M.K. Seo, J.R. Lee, S.J. Park, Crystallization kinetics and interfacial behaviors of polypropylene composites reinforced with multi-walled carbon nanotubes, Mater. Sci. Eng. A 404 (2005) 79–84, doi:10.1016/j.msea.2005.05.065.

[11] Q. Zhao, H.D. Wagner, D. Wagner, T. Raman, Raman spectroscopy of carbon-nanotube-based composit, Philos. Trans. R. Soc. A Math. Phys. Eng. Sci. 362 (2004) 2407–2424, doi:10.1016/S0140-6736(02)10308-4.

[12] D. Bikiaris, A. Vassiliou, K. Chrissafis, K.M. Paraskevopoulos, A. Jannakoudakis, A. Docoslis, Effect of acid treated multi-walled carbon nanotubes on the mechanical, permeability, thermal properties and thermo-oxidative stability of isotactic polypropylene, Polym. Degrad. Stab. 93 (2008) 952–967, doi:10.1016/j.polymdegradstab.2008.01.033.

[13] K. Chrissafis, K.M. Paraskevopoulos, S.Y. Stavrev, A. Docoslis, A. Vassiliou, D.N. Bikiaris, Characterization and thermal degradation mechanism of isotactic polypropylene/carbon black nanocomposites, Thermochim. Acta. 465 (2007) 6–17, doi:10.1016/j.tca.2007.08.007.

[14] G. Marosi, A. Márton, A. Szép, I. Csontos, S. Keszei, E. Zimonyi, A. Toth, X. Almeras, M.Le Bras, Fire retardancy effect of migration in polypropylene nanocomposites induced by modified interlayer, Polym. Degrad. Stab. 82 (2003) 379–385, doi:10.1016/S0141-3910(03)00223-4.

[15] N. Grossiord, M.E.L. Wouters, H.E. Miltner, K. Lu, J. Loos, B. Van Mele, C.E. Koning, Isotactic polypropylene/carbon nanotube composites prepared by latex technology: electrical conductivity study, Eur. Polym. J. 46 (2010) 1833–1843, doi:10.1016/j.eurpolymj.2010.06.009.

[16] G.V. Aldica, M.L. Ciurea, D.M. Chipara, A.M. Lepadatu, K. Lozano, I. Stavarache, S. Popa, M. Chipara, Isotactic polypropylene-vapor grown carbon nanofibers composites: electrical properties, J. Appl. Polym. Sci. 134 (2017) 45297, doi:10.1002/app.45297.

[17] I. Caretti, I. Jiménez, S. Van Doorslaer, Chemical changes in irradiated polypropylene studied by X-ray photoabsorption and advanced EPR/ENDOR spectroscopies, Eur. Polym. J. 53 (2014) 223–229, doi:10.1016/j.eurpolymj.2014.01.032.

[18] L. Feng, N. Xie, J. Zhong, J.M, Resources, Carbon nanofibers and their composites: a review of synthesizing, properties, and applications, Materials (2014) 3919–3945 (Basel), doi:10.3390/ma70x000x.

[19] J. Li, Z. Zhu, T. Li, X. Peng, S. Jiang, L.S. Turng, Quantification of the Young's modulus for polypropylene: influence of initial crystallinity and service temperature, J. Appl. Polym. Sci. 137 (2020) 1–7, doi:10.1002/app.48581.

[20] K. Tsobkallo, A. Tikhomirov, A. Tshmel, Intrafibrillar bridging structures in strained isotactic polypropylene, Polymer (Guildf). 45 (2004) 1689–1696. doi:10.1016/j.polymer.2003.12.054.

[21] H.D. WAGNER, M.S. AMER, L.S. Schadler, Residual compression stress profile in high-modulus carbon fiber embedded in isotactic polypropylene by micro-raman spectroscopy, Appl. Compos. Mater 7 (2000) 239–248, doi:10.1023/A:1008956929081.

[22] D.M. Chipara, D.M. Panaitescu, K. Lozano, R.A. Gabor, C.A. Nicolae, M. Chipara, Raman spectroscopy and molecular bases of elasticity: sEBS-graphite composites, Polymer 176 (2019) 74–88 (Guildf), doi:10.1016/j.polymer.2019.05.019.

[23] D.M. Chipara, C. Secu, K. Lozano, M. Secu, M. Chipara, C.A. Nicolae, M. Chipara, D.M. Chipara, C. Secu, K. Lozano, M. Secu, M. Chipara, Raman investigations on gamma irradiated iPP-VGCNF nanocomposites: the polymer's tale, Surfaces Interfaces 17 (2019) 100351, doi:10.1016/j.surfin.2019.100351.

[24] D.M. Chipara, A.C. Chipara, M. Chipara, Raman spectroscopy of carbonaceous materials: a concise review, Spectrosc. 26 (2011) 2–7 (Santa Monica).

[25] M.S. Dresselhaus, G. Dresselhaus, A. Jorio, A.G.S. Filho, R. Saito, A.G. Souza Filho, R. Saito, Raman spectroscopy on isolated single wall carbon nanotubes, Carbon N. Y. 40 (2002) 2043–2061, doi:10.1016/S0008-6223(02)00066-0.

[26] C. Thomsen, S. Reich, Raman scattering in carbon nanotubes, 232 (2007) 115–232.

[27] C.C. Chang, C.C. Chen, W.H. Hung, I.K. Hsu, M.A. Pimenta, S.B. Cronin, Strain-induced D band observed in carbon nanotubes, Nano Res. 5 (2012) 854–862, doi:10.1007/s12274-012-0269-3.

[28] M. Mu, S. Osswald, Y. Gogotsi, K.I. Winey, An in situ Raman spectroscopy study of stress transfer between carbon nanotubes and polymer, Nanotechnology (2009) 20, doi:10.1088/0957-4484/20/33/335703.

[29] Z. Liu, J. Zhang, B. Gao, Raman spectroscopy of strained single-walled carbon nanotubes, Chem. Commun. (2009) 6902–6918, doi:10.1039/b914588e.

[30] K. Kunc, I. Loa, K. Syassen, Equation of state and phonon frequency calculations of diamond at high pressures, Phys. Rev. B Condens. Matter Mater. Phys. 68 (2003) 1–9, doi:10.1103/PhysRevB.68.094107.

[31] G.A. Kourouklis, J. Arvanitidis, D. Christofilos, S. Ves, High pressure Raman spectroscopy in carbon nanotubes, Acta Phys. Pol. A 116 (2009) 13–18, doi:10.12693/APhysPolA.116.13.

[32] A.J. Ghandour, I.F. Crowe, J.E. Proctor, Y.W. Sun, M.P. Halsall, I. Hernandez, A. Sapelkin, D.J. Dunstan, Pressure coefficients of Raman modes of carbon nanotubes resolved by chirality: environmental effect on graphene sheet, Phys. Rev. B Condens. Matter Mater. Phys. 87 (2013) 1–5, doi:10.1103/PhysRevB.87.085416.

[33] F. Occelli, P. Loubeyre, R. Letoullec, Properties of diamond under hydrostatic pressures up to 140GPa, Nat. Mater. 2 (2003) 151–154, doi:10.1038/nmat831.

[34] I. Loa, Raman spectroscopy on carbon nanotubes at high pressure, J. Raman Spectrosc. 34 (2003) 611–627, doi:10.1002/jrs.1035.

[35] M. Hulman, V. Skákalová, S. Roth, H. Kuzmany, Raman spectroscopy of single-wall carbon nanotubes and graphite irradiated by γ rays, J. Appl. Phys. 98 (2005) 1–5, doi:10.1063/1.1984080.

[36] M.E. Sullivan, D. Klosterman, G.R. Palmese, Electron beam modification and functionalization of MWNT for covalent dispersion into polymeric systems, Nucl. Instrum. Methods Phys. Res. B 265 (2007) 352–355, doi:10.1016/j.nimb.2007.09.002.

[37] P.S.R. Sreekanth, N.N. Kumar, S. Kanagaraj, Improving post irradiation stability of high density polyethylene by multi walled carbon nanotubes, Compos. Sci. Technol. 72 (2012) 390–396, doi:10.1016/j.compscitech.2011.11.031.

[38] M.C. Evora, D. Klosterman, K. Lafdi, L. Li, J.L. Abot, Functionalization of carbon nanofibers through electron beam irradiation, Carbon N. Y. 48 (2010) 2037–2046, doi:10.1016/j.carbon.2010.02.012.

[39] O. Lourie, H.D. Wagner, O. Lourie, H.D. Wagner, Introduction, evaluation of young's modulus of carbon nanotubes by micro-raman spectroscopy, J. Mater. Res. 13 (1998) 2418–2422, doi:10.1007/springerreference_30108.

[40] B.P.M. Ajayan, L.S. Schadler, C. Giannaris, A. Rubio, Single-walled carbon nanotube ± polymer composites : strength and weakness **, Adv. Mater. 12 (2000) 750–753.

[41] P. Kannan, S.J. Eichhorn, R.J. Young, Deformation of isolated single-wall carbon nanotubes in electrospun polymer nanofibres, Nanotechnology 18 (2007), doi:10.1088/0957-4484/18/23/235707.

[42] M.A. de Baez, P.J. Hendra, M. Judkins, The Raman spectra of oriented isotactic polypropylene, Spectrochim. Acta Part A 51 (1995) 2117–2124, doi:10.1038/144438b0.

[43] K. Bocz, K.E. Decsov, A. Farkas, D. Vadas, T. Bárány, A. Wacha, A. Bóta, G. Marosi, Non-destructive characterisation of all-polypropylene composites using small angle X-ray scattering and polarized Raman spectroscopy, Compos. Part A Appl. Sci. Manuf. 114 (2018) 250–257, doi:10.1016/j.compositesa.2018.08.020.

[44] A.S. Nielsen, D.N. Batchelder, R. Pyrz, Estimation of crystallinity of isotactic polypropylene using Raman spectroscopy, Polymer 43 (2002) 2671–2676 (Guildf), doi:10.1016/S0032-3861(02)00053-8.

[45] G.V. Fraser, P.J. Hendra, D.S. Watson, M.J. Gall, H.A. Willis, M.E.A. Cudby, The vibrational spectrum of polypropylene, Spectrochim. Acta Part A Mol. Spectrosc. 29 (1973) 1525–1533, doi:10.1016/0584-8539(73)80216-8.

[46] M.C. Tobin, The infrared spectra of polymers. III. The infrared and Raman spectra of isotactic polypropylene, J. Phys. Chem. 64 (1960) 216–219, doi:10.1021/j100831a007.

[47] T. Kida, Y. Hiejima, K. Nitta, Raman spectroscopic study of high-density polyethylene during tensile deformation, Int. J. Exp. Spectrosc. Tech. 1 (2016) 1–6, doi:10.35840/2631-505x/8501.

[48] S. Prawer, R.J... Nemanich, R.J... Nemanic, R.J. Nemanich, R.J., Nemanic, Raman spectroscopy of diamond and doped diamond, Philos. Trans. Math. Phys. Eng. Sci. 362 (2004) 2537–2565.

[49] J. Yu, T.E. Lacy, H. Toghiani, C.U. Pittman, Effective property estimates for composites containing multiple nanoheterogeneities: part I nanospheres, nanoplatelets, and voids, J. Compos. Mater. 47 (2013) 549–558, doi:10.1177/0021998312442557.